ELSEVIER

Computers in Biology and Medicine ▮▮▮ (▮▮▮▮) ▮▮▮–▮▮▮

Computers in Biology and Medicine

www.intl.elsevierhealth.com/journals/cobm

Compartmental models of mammalian motoneurons of types S, FR and FF and their computer simulation

M.F. Vieira[a], A.F. Kohn[b,*]

[a]*Faculdade de Educação Física, Universidade Federal de Goiás, Brazil*

[b]*Biomedical Engineering Laboratory and Neuroscience Program, Universidade de São Paulo, Escola Politécnica, PTC, CEP 05508-970 São Paulo, SP, Brazil*

Received 12 December 2005; received in revised form 23 August 2006; accepted 6 September 2006

Abstract

Mathematical models of motoneurons (MNs) of types S, FR and FF were developed based on cat MN data. Each of the three models has an initial segment, a soma and a dendritic tree. The initial segment and the soma include models of several types of ionic currents, including a calcium-dependent slow potassium current. The dendritic tree is modeled as a series association of several electrically passive cylinders. Afterhyperpolarization parameters, current to frequency relation and the responses to input current steps, ramps and sinusoids were used for model validation. The effects of sinusoidally varying synaptic inputs at different levels of the dendritic tree were studied by computer simulation. The corresponding frequency response functions resulted of lowpass type with cutoff frequencies from 10 to 40 Hz, for synapses occurring more distally or more proximally, respectively. The nonlinear effects caused by two sinusoidally varying synaptic conductances (at 7 and 11 Hz), acting at different dendritic segments, were quantified by spectral analysis of the current reaching the soma. The simulations pointed to two main nonlinear effects: (i) harmonics of the two input frequencies (e.g., 14 Hz) and (ii) intermodulation terms (e.g., 4 Hz). When the two synaptic inputs occurred on more distal dendritic compartments the nonlinear effects were more pronounced.

Keywords: Motoneuron; Mathematical model; Motoneuron model; Computational model; Model validation; Compartmental models; Dendritic processing

1. Introduction

The motoneurons (MNs) are the elements of the central nervous system (CNS) that provide the link between the commands generated by the nervous system and the muscle fibers. The link they provide is not a mere relay, but a rather sophisticated signal processor. The static and dynamic behaviors of MNs are relevant in defining the "language" employed by the CNS to control the muscles. Due to the complexity of MNs and the neuronal networks in which they are embedded, many questions about their roles and the ways they are controlled by the CNS require a more theoretical approach, either by analytical methods or by computer simulations of mathematical models. The latter are warranted when medium to high-complexity MN models are the center of the study, which is the case in the present paper.

Vertebrate MN models started being developed at least 40 years ago [1], for different purposes. Biophysically realistic, rather complex, MN models have been developed to mimic many of the experimentally found motoneuronal characteristics [2–8]. These models were developed for the study of a wide range of phenomena at the neuronal level. Other less complex models were also developed with the objective of answering simpler or more focused questions [9–14]. Finally, MN models have also been developed when the behavior of an MN pool and the muscle it innervates was the focus of the study [15–19].

The objective of the present work was to develop mathematical models of mammalian MNs to be used in (a) studies of the behavior of single MNs subjected to different physiological conditions, (b) studies of MN pools subjected to a variety of descending and afferent synaptic commands. A particular application of the latter case is in the interpretation of experimental results obtained from humans to elucidate the functioning of the spinal cord neuronal circuitry [17,19,20]. Due to the

* Corresponding author. Tel.: +55 11 3091 5535; fax: +55 11 3091 5718.
E-mail address: andfkohn@leb.usp.br (A.F. Kohn).

0010-4825/$ - see front matter © 2006 Published by Elsevier Ltd.
doi:10.1016/j.compbiomed.2006.09.001

large numbers of neurons involved, the MN models to be used in such studies have to combine biological reality with computational efficiency.

Motor units in humans and higher animals are usually composed of a mixture of three main types, S, FR and FF [21]. This division in three types is often employed in the literature and refers mainly to the properties of the muscle fibers innervated by each MN. The MNs have characteristics that are related to the motor unit type, even though it is known that there may be some overlap in the values of many parameters [21–24]. One important characteristic is the afterhyperpolarization (AHP) that follows the discharge of an action potential. The AHP in MNs is quite pronounced and has a long duration, contributing to the relative refractory period and to a limitation of the maximum firing rate [25]. Many of the dynamic properties of MNs depend strongly on mechanisms behind the generation of the AHP. Another important quantifier of MN behavior is the f/I relation. When a constant current is injected in an MN, its steady-state firing rate f increases with an increase in the current intensity I. Different MN types exhibit a different f/I relation. The features of the mapping from the injected current I to the firing rate f are important from a functional standpoint because an increase in the MN firing rate will cause an increase in the force generated by the muscle fibers innervated by that MN [26]. The modeling effort in this work was oriented towards the development of three different MN models, each one being a sort of representative of each of the three main types of MNs.

This contribution builds on the model developments of previous scientists. Several MN models have evolved during the lifespan of neuroscience, their creation being guided by different assumptions and objectives. We chose one evolutionary branch that leads to biologically realistic mathematical models but with a complexity level that could allow their use in a computer simulator of an MN pool.

For the validation of our mathematical models of MNs we chose a *battery of tests* that covered both static and dynamic conditions. The latter aspect is of special relevance because most published MN models have been validated with a quite restricted set of tests, mostly for constant current inputs.

2. Methods

The following topics will be covered in this section: (i) development of S, FR and FF models; (ii) battery of tests for MN model validation.

The three mathematical models were encoded in C++ language and run in a Windows environment. This assured a fast simulation time as compared with available general purpose neuronal simulators such as Genesis, Nodus or Neuron. Nevertheless, the greatest advantage of such an implementation is that the resulting code can be embedded in any MN pool simulator written in C++. The parameter values for the three models are available at www/leb.usp.br/MNs.

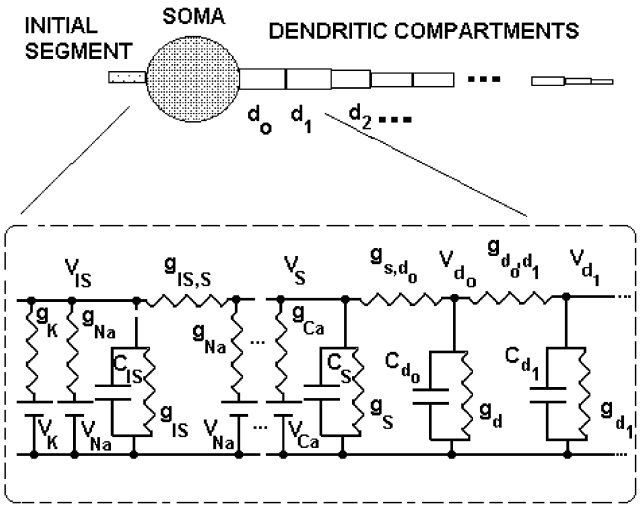

Fig. 1. General schematic of each motoneuron model. The electrical equivalent circuits for the soma, the initial segment and the first two dendritic compartments are shown. The soma and the initial segment are each modeled by parallel associations of a capacitance and several voltage-dependent conductances (only few are shown), each in series with a battery.

2.1. Development of the S, FR and FF models

The S and FR MN models departed from the respective models developed in [3]. Our models ended up containing some different ionic currents. To complete the set, a model for type FF MNs was also developed. The battery of tests, to be presented below, was applied to several of the existing MN models and the results gave several clues as to the types of required improvements, either pointing to the need for other types of ionic channels or for different parameter values.

2.1.1. General MN model structure

The general structure of each of the developed models is shown in Fig. 1, where the electrical equivalent of the initial segment, the soma and the first two dendritic compartments is indicated. Each dendritic compartment (d_i) is represented as a cylinder, the soma (S) is represented as an equivalent sphere and the initial segment (IS) is represented as a cylinder. The geometric and basic electrical parameters for each of the three models are given in the Appendix. The differential equations relating the membrane potentials of neighboring dendritic compartments arise naturally from the electrical circuit of the equivalent dendritic cable (Fig. 1).

2.1.2. General model for the somas

To mimic real MNs [27], the mathematical model of the soma represents several ionic currents, indicated by I_{ions} in the equation below, that are associated with different voltage-dependent ionic conductances. In addition, the soma receives a current from the first dendritic segment (d_0) and another current from the initial segment, which depend on the coupling conductances g_{S,d_0} and $g_{S,\text{IS}}$. Therefore, the general differential equation relating the soma membrane potential to the

Please cite this article as: M.F. Vieira, A.F. Kohn, Compartmental models of mammalian motoneurons of types S, FR and FF and their computer simulation, Comp. Biol. Med. (2006), doi: 10.1016/j.compbiomed.2006.09.001

Table 1
Geometric and electrical data of the soma of the proposed models

	Type S	Type FR	Type FF
Geometric data			
Diameter of the soma (μm)	50.9	48.8	49.2
Area of the soma (μm^2)	7569.86	6146.34	6564.01
Electrical data			
Specific membrane capacitance (μF/cm^2)	1.0	1.0	1.0
Specific membrane resistivity at soma (Ω cm^2)	700	225	70
Specific cytoplasmic resistivity (Ω cm)	70	70	70
Membrane conductance (mS)	1.08×10^{-4}	2.73×10^{-4}	8.49×10^{-4}
Membrane capacitance (μF)	7.57×10^{-5}	6.15×10^{-5}	6.56×10^{-5}

above-mentioned currents is

$$C_S \frac{dV_S}{dt} = I_{ions} + g_{S,d_0}(V_{d_0} - V_S) + g_{S,IS}(V_{IS} - V_S) + g_{L,S}(E_{L,S} - V_S),$$

where V_S is the soma membrane potential, C_S is the soma membrane capacitance, g_{S,d_0} is the coupling conductance between the soma and dendritic compartment d_0, V_{d_0} is the membrane potential at the dendritic compartment d_0, $g_{S,IS}$ is the coupling conductance between the initial segment and the soma, V_{IS} is the membrane potential of the initial segment, $g_{L,S}$ is the leakage conductance and $E_{L,S}$ is the resting membrane potential. The ionic currents I_{ions} in the soma are composed of fast sodium and potassium currents $I_{Na(soma)}$ and $I_{Kf(soma)}$, slow potassium currents $I_{BKs(soma)}$ and $I_{SKs(soma)}$ and calcium currents of types N and L. Their equations are given in detail in the Appendix. A similar equation describes the initial segment, except that it does not have the current input from dendritic compartment d_0 and it has fewer types of ionic channels, as will be shown later.

The soma of each MN model (of types S, FR and FF) was modeled as a sphere, with diameter 50.9 μm for type S MN model, 48.8 μm for type FR and 49.2 μm for type FF. The specific membrane resistivity was 700, 225 and 70 Ω cm^2 in the soma for the S, FR and FF MN, respectively. For all models, the specific membrane capacitance was 1.0 μF/cm^2 and the specific cytoplasmic resistivity was 70 Ω cm. The respective membrane leakage conductances were 1.08×10^{-4}, 2.73×10^{-4} and 8.49×10^{-4} mS while the membrane capacitances were 7.57×10^{-5}, $6.15 \times 10^{-5}$and 6.56×10^{-5} μF (Table 1).

The geometric and electrical data of the soma are summarized in Table 1.

2.1.3. Models for the dendritic trees

The geometries of the equivalent dendritic trees for the S and FR models were similar to those employed in [3], with experimental data taken from [28,29]. Their experimental data from cat triceps surae MNs provided the basis for the development of the equivalent cables, more specifically, MNs 35/4 and 43/5 served as templates for the S and FR MN models. The first compartment of the S (FR) MN equivalent dendrite had a 25 μm (40 μm) diameter and a 500 μm (500 μm) length. The final compartment had a 0.63 μm (1.0 μm) diameter and a 125 μm (100 μm) length. There were 17 (19) compartments with a total length of 7000 μm(6675 μm) in the S (FR) MN model equivalent dendritic cable, both ending with a sealed end, with an electrotonic length of 2.29λ (2.448λ). The passive dendritic parameters were taken from [29] using the step model: specific membrane resistivity 20 000 Ω cm^2 (11 000 Ω cm^2) in the dendrites. For both models, the specific membrane capacitance was 1.0 μF/cm^2 and the specific cytoplasmic resistivity was 70 Ω cm. The conductance and capacitance values of the dendritic models for S and FR MNs may be found in the Appendix.

To construct the type FF MN dendritic model we used experimental results from neuron 41/2 described in [28,29]. The equivalent tapering cable resulted with a total length of 6650 μm with an electrotonic length of 1.96λ. This length was represented by 19 compartments in a row, the first with 35 μm in diameter and 500 μm in length, and the last with 0.5 μm in diameter and 100 μm in length. The passive dendritic parameters were taken from [29] using the step model: specific membrane resistivity 20 000 Ω cm^2 in the dendrites. The specific membrane capacitance was 1.0 μF/cm^2 and the specific cytoplasmic resistivity was 70 Ω cm. The dendritic compartment parameters of the FF MN model may be found in the Appendix.

The geometric and electrical data of the dendrites are summarized in Table 2.

2.1.4. Models for the initial segments

As in [3], the initial segment was modeled as a single compartment equivalent to a cylinder of diameter 10 μm and length 100 μm for the three MN models, its leakage conductance in parallel with the axonal equivalent input resistance represented by conductance g_{IS}. As the specific membrane resistivity was different for the S, FR and FF models (see above), the equivalent membrane conductance was different in each: 4.6×10^{-5}, 1.43×10^{-4} and 4.16×10^{-4} mS, respectively. However, as the areas of the initial segments were equal in the three models, the equivalent membrane capacitances were 3.22×10^{-5} μF in all three (Table 3). The voltage-dependent channels were modeled as done in [2,4]. These consisted of the classic Na and K fast channels, similar for the three models, with parameter values that made the firing threshold in the initial segment lower than in the soma (the expressions are given in the Appendix).

Please cite this article as: M.F. Vieira, A.F. Kohn, Compartmental models of mammalian motoneurons of types S, FR and FF and their computer simulation, Comp. Biol. Med. (2006), doi: 10.1016/j.compbiomed.2006.09.001

Table 2
Geometric and electrical data of the dendrites of the proposed models

	Type S	Type FR	Type FF
Geometric data			
Number of compartments	17	19	19
First compartment diameter (μm)	25	40	35
First compartment length (μm)	500	500	500
Final compartment diameter (μm)	0.63	1.0	0.5
Final compartment length (μm)	125	100	100
Electrical data			
Specific membrane resistivity at dendrites ($\Omega\,cm^2$)	20 000	11 000	20 000
Specific membrane capacitance ($\mu F/cm^2$)	1.0	1.0	1.0
Specific cytoplasmic resistivity ($\Omega\,cm$)	70	70	70
Total length of the equivalent dendrite (μm)	7000	6675	6650
Electrotonic length	2.29λ	2.448λ	1.96λ

Table 3
Geometric and electrical data of the initial segment of the proposed models

	Type S	Type FR	Type FF
Geometric data			
Length of the initial segment (μm)	100	100	100
Diameter of the initial segment (μm)	10	10	10
Area of the initial segment (μm^2)	3220.13	3220.13	3220.13
Electrical data			
Specific membrane capacitance ($\mu F/cm^2$)	1.0	1.0	1.0
Specific membrane resistivity at initial segment ($\Omega\,cm^2$)	700	225	70
Specific cytoplasmic resistivity ($\Omega\,cm$)	70	70	70
Membrane conductance (mS)	4.6×10^{-5}	1.43×10^{-4}	4.16×10^{-4}
Membrane capacitance (μF)	3.22×10^{-5}	3.22×10^{-5}	3.22×10^{-5}

The geometric and electrical data of the initial segment are summarized in Table 3.

2.1.5. Details of the models for the somas

For the S and FR models we started out from the models in [3] and hence our initial task was to replicate their results. We were successful with the S-type MN model, but could not replicate the simulation results of their FR model. After exhaustive trials, we discovered that we could replicate their results for the FR model if we used the specific membrane resistivity values *of the* S*-type MN* for the soma and initial segment of the FR model. However, when we used the correct resistivity values for the FR MN and the values given in their paper of the ionic channel dynamics, our simulation results did not fit their results and neither the values reported in the experimental literature on MNs. The fast Na^+ and K^+ channels were modeled as done in [3], which are slight modifications of Traub's models [4,5]. As the FR model in [2] did not fit adequately basic MN data (due to the problem we mentioned before) and as both their S and FR models could not replicate experimental data on the dynamic properties of MNs (e.g., pattern of spiking for ramp and sinusoidal injected currents), we thought that a more biophysically realistic representation of the slow K^+ current could yield substantial improvements. Therefore, their slow K^+ current was replaced by two slow K^+ currents that depended explicitly on intracellular Ca^{2+} concentration, the first being a type SK current and the second a BK current [30]. Two types of Ca^{2+} current, types N and L, contributed to the variations in intracellular Ca^{2+} concentration. All these different ionic currents will be described explicitly in separate subsections because they are a major departure from previous work on MNs and many of the improvements achieved by the new models are due to the introduction of such currents. Jones and Bawa [2] did not model FF MNs, but Traub [4] did, so we ran his FF-type MN model through our battery of tests described above. Unfortunately, his model suffered from inadequate behavior in dynamic tests such as injection of ramp and sinusoidal currents [31]. Therefore, also for the FF MN model, major departures from existing models had to be chosen for improved representation of real MN behavior.

2.1.6. Models for the somatic calcium currents

The somatic calcium currents are important in MNs with respect to the slow calcium-dependent potassium currents while they exert little direct influence on the action potential itself. The N-type Ca^{2+} current was modeled as done in [13], but with changes in some parameter values: $I_{CaN} = g_{max} m_N^2 h_N (V_m - E_{Ca})$, with $g_{max} = 2.00\,mS/cm^2$ for type S MN, $g_{max} = 2.13\,mS/cm^2$ for FR MN, $g_{max} = 2.00\,mS/cm^2$ for FF MN and $E_{Ca} = 140\,mV$. The membrane potential and the ionic equilibrium potentials represent variations about the resting potential. The activation and inactivation state variables

Please cite this article as: M.F. Vieira, A.F. Kohn, Compartmental models of mammalian motoneurons of types S, FR and FF and their computer simulation, Comp. Biol. Med. (2006), doi: 10.1016/j.compbiomed.2006.09.001

m_N and h_N were described by a standard first order differential equation $dx/dt = (x_\infty - x)/\tau$, where x stands for either state variable, with the following steady-state functions and time constants, equal for the three types of MNs:

$$m_N: m_{N\infty} = \frac{1}{1 + e^{((V_m - 40)/-5)}},$$

$$\tau_{m_N} = 4\,\text{ms},$$

$$h_N: h_{N\infty} = \frac{1}{1 + e^{((V_m - 25)/10)}},$$

$$\tau_{h_N} = 40\,\text{ms}.$$

The model structure for the L-type Ca^{2+} current was similar to that used in [12], but with the activation variable squared, as done in [32], and with a larger time constant (but still within physiological limits). This turned out to be necessary for a better reproduction of the cat MN AHP time course and a better reproduction of the firing rate adaptation (early phase) found in the cat literature. The current was described by $I_{CaL} = g_{max} m_L^2 (V_m - E_{Ca})$, with $g_{max} = 2.60\,\text{mS/cm}^2$ for type S MN, $g_{max} = 2.67\,\text{mS/cm}^2$ for FR MN, $g_{max} = 2.50\,\text{mS/cm}^2$ for FF MN and $E_{Ca} = 140\,\text{mV}$. The activation state variable m_L was described by the same type of first order differential equation as above for the N-type current, with the following steady-state function and time constant, equal for the three types of MNs:

$$m_{L\,inf} = \frac{1}{1 + e^{((V_m - 25)/-5)}},$$

$$\tau_{m_N} = 40\,\text{ms}.$$

2.1.7. Calcium concentration in the cytoplasm

Several possibilities of modeling the relation between the calcium concentration and the calcium current were tried out by running exhaustive simulations. The best results were obtained by the proposal described in [5], but with a change in the value of β_q:

$$\frac{d[Ca^{+2}]}{dt}(\text{mmol/l/ms}) = \frac{c}{A\delta} I_{Ca}(10^3\,\text{C/l/ms}) - \beta_q [Ca^{+2}](\text{mmol/l/ms})$$

with $c = 400\,\text{mmol}/10^3\,\text{C}$, $\delta = 2 \times 10^{-4}\,\mu\text{m}$ and $\beta_q = 0.10\,\text{m/s}$ ($\beta_q = 0.09\,\text{m/s}$ for type S MN). For each MN type, the respective soma area A is to be employed in the equation above.

2.1.8. Slow, calcium-dependent, potassium current of type SK

This type of low-conductance calcium-dependent potassium channel is discussed in [30] and its current, included only in the soma, was modeled here by $I_{SKs(soma)} = g_{max}([Ca^{2+}]/K_d)^2(V_m - E_K)$, with $E_K = -10\,\text{mV}$ and $g_{max} = 3.00\,\text{mS/cm}^2$, $K_d = 0.15$ for the type S MN model, $g_{max} = 23.40\,\text{mS/cm}^2$, $K_d = 0.50$ for the type FR MN model and $g_{max} = 22.00\,\text{mS/cm}^2$, $K_d = 0.80$ for the type FF MN model. It is very sensitive to higher calcium concentrations, its saturation depending only on the saturation of calcium in the cytoplasm. In developing the MN models, we initially only included this slow potassium current but the results were not good. For example, for injected step currents the first interspike interval was longer than the following ones; above certain constant input current amplitudes there were oscillations in the interspike intervals (both behaviors being atypical of MNs in normal conditions). The addition of another slow potassium current, the BK type, conferred the appropriate dynamics to the MN models.

2.1.9. Slow, calcium-dependent, potassium current of type BK

This current, also included only in the soma, was modeled with a voltage dependence that is structurally similar to the slow potassium current described in [2,4] but with an added explicit calcium dependence, which was adapted from [32]: $I_{BKs(soma)} = g_{max} q^2 r (V_m - E_K)$. For the types S, FR and FF MNs, the values of g_{max} were 9.00, 35.00 and 32.00 mS/cm^2 and $E_K = -10\,\text{mV}$. The activation variable was described by $dq/dt = \alpha_q(1 - q) - \beta_q$, where

$$\alpha_q = \frac{3.5}{e^{((V_m - 45)/-4)} + 1} \quad \text{for the three of MNs,}$$

$$\beta_q = \frac{\beta_{num}}{e^{((V_m + 50)/-0.001)} + 1} \quad \text{with } \beta_{num} = 0.018,$$

0.042 and 0.048 for the types S, FR and FF MNs, respectively, and

$$r = \frac{[Ca^{2+}]}{[Ca^{2+}] + \theta} \quad \text{with } \theta = 0.4$$

for types S and FR MNs and $\theta = 0.2$ for type FF.

The voltage sensitivity of this current had to be increased [30] from the original Jones and Bawa formulation in [2] and, therefore, the steady-state curve of the activation variable was shifted to the left by 10 mV. Due to the steep sigmoidal curve, the activation variable squared q^2 remains near zero for membrane potentials below threshold and increases fast to maximal activation around threshold. Therefore, the conductance is activated by an action potential and decays with an exponential time course. The calcium dependence of this current is described by a rather steep curve, according to what has been described experimentally [30]. Therefore, as the activation variable r easily reaches values near 1 for small calcium concentrations, the voltage dependence of this modeled BK-type channel usually prevails. The interplay of the dynamics of the two types of calcium-dependent potassium currents was able to improve the reproduction of many behaviors observed in real MNs, as will be shown in Results.

2.1.10. Synaptic inputs

Excitatory synaptic inputs generated synaptic currents modeled by $I_{syn}(t) = g_{syn}(t) * (V_m - E_{syn})$, where $E_{syn} = 70\,\text{mV}$ and $g_{syn} = g_{max} t e^{-t/\tau}$, with $t = 0.2\,\text{ms}$. For computational convenience in applications with trains of presynaptic inputs activating the dendritic synapses, the synaptic conductance in each dendritic compartment was simulated as the impulse response of a second order linear system. The value of g_{max} in a given dendritic compartment was given by the peak conductance of a

Please cite this article as: M.F. Vieira, A.F. Kohn, Compartmental models of mammalian motoneurons of types S, FR and FF and their computer simulation, Comp. Biol. Med. (2006), doi: 10.1016/j.compbiomed.2006.09.001

Table 4
Free and fixed parameters in model tuning

Free parameters (or variables)	Fixed parameters (or variables)
g_{maxBK} (maximal conductance for slow potassium current type BK)	Maximal conductance for all currents except for those in the first column
g_{maxSK} (maximal conductance for slow potassium current type SK)	All variables α and β, except for those in the first column
g_{maxCaN} (maximal conductance for calcium current type N)	All membrane capacitances
g_{maxCaL} (maximal conductance for calcium current type L)	All coupling conductances
β_q (state variable for slow potassium current type BK)	All membrane conductances
K_d (constant related to slow potassium current type SK)	

single synaptic contact times the number of synaptic contacts on that dendritic compartment. In some simulations we wanted to study the effect of a sinusoidal variation in g_{syn} on the somatic current (i.e., the current entering the soma from the dendritic tree) and hence in such cases we imposed directly $g_{syn}(t) = A\cos(\omega_0 t)$.

2.1.11. Model tuning

The basic criteria for model adjustments were the minimization of the errors between simulated and real MN data with respect to the AHP and the f/I relation simultaneously, with a secondary priority given to the time course of the firing rate adaptation. Experiments in cat MNs have shown that their f/I curves are approximately linear, with the possibility of a higher slope secondary linear range occurring mainly for S-type MNs discharging steadily at higher rates (above several dozens of action potentials/s) [26]. The secondary range may be caused by the activation of a persistent current due to the increase in firing threshold at higher discharge rates [33]. From a functional point of view the primary range seems to be the most important since it is associated with the highest sensitivity of force development by the muscle units [26]. Additionally, the higher firing rates associated with the secondary range (at least in S-type MNs) do not seem to occur in humans [34,35]. Therefore, in the present work the focus was on the appropriate reproduction of the f/I relation in the primary firing range of real MNs.

After the final model structure was arrived at, several parameters were adjusted to decrease the fitting errors. The AHP amplitude could be adjusted by varying the density of slow K^+ channels in the soma, but also by changing the Ca^{2+} channel density in the soma, or both. Within this context four parameter values could be altered to obtain the desired AHP amplitude: the maximum conductances of the BK and SK potassium currents and those of the N- and L-type calcium channels. This task, nevertheless, was not that easy because if improper parameter values were used, the calcium currents could alter significantly the action potential time course. Initially, maximum Ca^{2+} conductances were determined so that a desired firing rate adaptation occurred while causing a calcium concentration that indirectly would yield desired slow potassium currents. After these adjustments, the slow potassium maximum conductance values could be changed until a desired AHP peak value was reached. On the other hand, the AHP duration and time for half decay could be adjusted by the constant K_d of the SK potassium current and by variable β_q of the BK potassium current. As soon as an adequate AHP was obtained, the slope of the f/I curve was estimated using a least squares algorithm. Many times a good result with the AHP did not correspond to a good f/I curve slope because the active currents do not have the same behavior for long depolarizations (used to find the f/I relation) as for short duration current stimuli (used for AHP fitting).

Some parameters, like the fast sodium and potassium conductances, were adjusted only once to reproduce the magnitude of the action potential described in the cat literature. Other parameters, like the geometry-dependent dendritic conductances and capacitances, were kept unaltered once they were computed. A synthesis of the free and fixed parameters involved in the model fitting is shown in Table 4.

2.2. Battery of tests for MN model validation

Both static and dynamic tests were included in the battery. The static tests are associated with the neuron at rest, or discharging either a single action potential (in response to a single current pulse) or a train of action potentials (recorded in steady state in response to a constant current injected at the soma). The dynamic tests involved cases where the input current amplitude varied with time: steps, ramps and sinusoids. The first would be an approximation to the resultant somatic currents of synaptic origin due to descending commands for a ballistic movement. The second mimics the equivalent somatic current for a gradually increasing muscle activation and the third mimics what should happen during rhythmic movements, like walking or running. We tried to follow similar procedures to those employed experimentally by researchers of MN physiology. Each of the tests is briefly described in what follows.

2.2.1. Input resistance

Hyperpolarizing input current pulses (50 ms) of three different amplitudes (1.0, 2.0 and 3.0 nA) were applied to the soma and the resulting membrane potential was measured at the pulse end. The input resistance was estimated by the slope of a straight line fitted to the three (I, V) values. Experimental values were taken from [29].

2.2.2. System time constant

Short (0.2 ms) hyperpolarizing current pulses were injected in the soma and the resulting membrane potential time course was plotted in semi-logarithmic scale to yield an estimate of the time constant, computed where the plot was already a straight line. Experimental values for comparison were taken from [29].

Please cite this article as: M.F. Vieira, A.F. Kohn, Compartmental models of mammalian motoneurons of types S, FR and FF and their computer simulation, Comp. Biol. Med. (2006), doi: 10.1016/j.compbiomed.2006.09.001

2.2.3. AHP parameters

An action potential was fired by a short (0.5 ms) current pulse injected in the soma, and the AHP peak amplitude, duration, time of half decay and time to peak were measured. Experimental values were taken from [24].

2.2.4. Tests using a constant current input

From these tests the rheobase, the minimum firing rate and the f/I curve could be evaluated. The rheobase was estimated as the smallest current intensity that for 50 ms could fire at least one action potential. The constant current value was increased until a steady repetitive firing pattern was obtained. This yielded the minimum firing rate. The f/I curve was obtained by plotting the mean discharge rate, measured after the firing rate reached a steady-state value, as a function of the injected current step amplitude. Experimental reference data were taken from [22,24,36].

2.2.5. Step current input

The firing rate usually decayed to a steady-state rate value. The firing rate adaptation was evaluated by plots of the instantaneous rate (inverse of each interspike interval) as a function of time. Experimental values for model validation were taken from [37].

2.2.6. Ramp current input

The instantaneous firing rate was plotted as a function of time for different ramp velocities. Actually the inputs were ramp-and-hold currents, so that the instantaneous firing rate was plotted during the ramp as well as during the plateau. Experimental values were taken from [23,38].

2.2.7. Sinusoidal current input

As the experimental reference data used in the models' validation came from Refs. [22,39], we followed their methodology. The input was a sinusoidal current superimposed on a step current, the latter setting up a basal firing rate. The sinusoidal current variation resulted in a quasi-sinusoidal firing rate variation of the neuron, with a gain and a phase that depended on the input sinusoidal frequency. The gain was estimated using a few different input amplitudes and measuring the resulting amplitudes of frequency modulation. For a given pair of input current frequency and amplitude, the instantaneous frequencies were computed from the ongoing neuronal spike train for many input cycles and used to build a cycle histogram. Peak instantaneous frequencies measured from the cycle histograms were plotted as a function of the input amplitude of the sinusoids. The slope of such a curve (spikes/s nA) was taken as the gain at that frequency while the phase was derived from an FFT.

3. Results

The simulation results of the three MN models will focus on their validation, i.e., we shall compare the model simulation results with those from real MNs as described in cat literature.

Table 5
Input resistance

	Type S (MΩ)	Type FR (MΩ)	Type FF (MΩ)
Proposed models	3.22	1.24	0.69
Fleshman et al. [29]	4.2	1.4	0.7
Gustaffson and Pinter [40]	[1.7–4.0]	[1.2–1.7]	[0.6–1.2]
Jones and Bawa [2] models	3.9	2.0	–
Traub's [4,5] models	2.0	1.5	1.0

Table 6
System time constant

	Type S (ms)	Type FR (ms)	Type FF (ms)
Proposed models	12.8	6.9	7.2
Fleshman et al. [29]	13.0	6.8	6.9
Jones and Bawa [2] models	16.4	8.8	–
Traub's [4,5] models	–	–	2.78

3.1. Input resistance

The resistance measured from the soma of the S, FR and FF models were 3.22, 1.24 and 0.69 MΩ, respectively. These values reproduce reasonably well experimental and simulation results from cat lumbar MNs: (i) the data for the 35/4, 43/5 and 41/2 MNs described in [29] were 4.2, 1.4 and 0.7 MΩ, respectively; (ii) the experimentally measured ranges for S, FR and FF cat lumbar MNs found in [40] were, approximately, 1.7–4.0, 1.2–1.7 and 0.6–1.2 MΩ, respectively. These results are summarized in Table 5.

3.2. System time constant

The system time constants for the S, FR and FF models resulted as 12.8, 6.9 and 7.2 ms, respectively. These values compare well with those reported in [29]: 13.0, 6.8 and 6.9 ms. The ranges found from cat lumbar experiments have a reasonable overlap [24,40], so this parameter is not a characteristic feature of different MN types. These results are summarized in Table 6.

3.3. AHP parameters

The S-type MN model presented a peak AHP value 6.18 mV, an AHP duration 164.50 ms and AHP half-decay time 33.57 ms. The corresponding values for the FR MN model were 4.28 mV, 78.77 ms and 18.02 ms, while for the FF they were 2.80 mV, 65.69 ms and 13.98 ms. These results are within the experimental ranges obtained from the cat. For example, the AHP durations measured from gastrocnemius MNs from 42 cats [24] were in the ranges 75–285, 45–150 and 30–135 ms, for the S, FR and FF types, respectively. These results are summarized in Table 7. The AHP waveforms are shown in Fig. 2.

Please cite this article as: M.F. Vieira, A.F. Kohn, Compartmental models of mammalian motoneurons of types S, FR and FF and their computer simulation, Comp. Biol. Med. (2006), doi: 10.1016/j.compbiomed.2006.09.001

Table 7
AHP parameters

	Type S			Type FR			Type FF		
	Mag. (mV)	Duration (ms)	$\frac{1}{2}$ Decay time (ms)	Mag. (mV)	Duration (ms)	$\frac{1}{2}$ Decay time (ms)	Mag. (mV)	Duration (ms)	$\frac{1}{2}$ Decay time (ms)
Proposed models	6.18	164.50	33.57	4.28	78.77	18.02	2.80	65.69	13.98
Zengel et al. [24]	4.9 ± 0.6 [1–9.5]	161 ± 14 [75–280]	44 ± 2 [19–60]	4.3 ± 0.4 [1–8.5]	78 ± 4 [45–140]	22 ± 1 [13–29]	3.0 ± 0.2 [1–7.5]	65 ± 2 [30–130]	18 ± 0 [19–29]
Jones and Bawa [2] models	4.8	160.0	48.04	4.1	90.0	23.0	–	–	–
Traub's [4,5] models	–	–	–	–	–	–	3.5	80.71	–

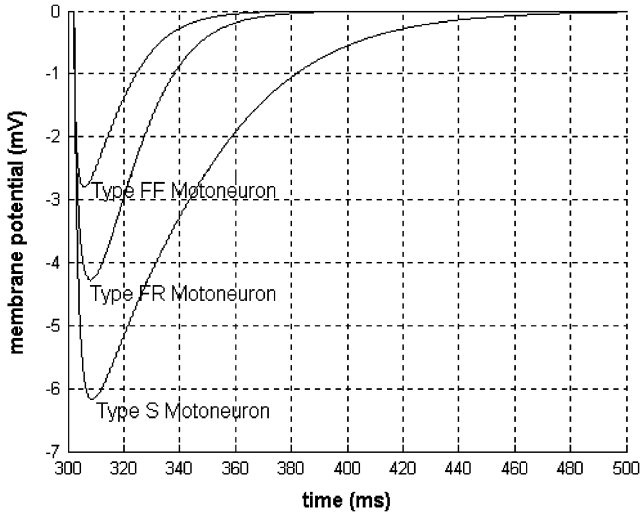

Fig. 2. Afterhyperpolarization (AHP) time courses that resulted from the simulations of the three motoneuron models.

3.4. Tests using a constant current input

The rheobase for the S, FR and FF models were 3.02, 8.20 and 19.09 nA, being within the ranges found for cat gastrocnemius MNs [24,40]. For example, from the data in [40] the approximate rheobase ranges were 1.2–8.0, 7.5–15.0 and 14.0–32.0 nA for the S, FR and FF MNs (Table 8).

A slightly higher constant input current to each MN model assured a steady discharge, with minimum rates 7.59, 13.45 and 15.48 spikes/s, for the S, FR and FF models, respectively. Even though the authors in [28,29] did not measure the minimum firing rates of the three MNs that were our prototypes for model building, the ordering of minimum rates from the S to the FF types and their values are compatible with findings from cat lumbosacral MNs [25,41]. The f/I relations for the S, FR and FF MN models showed slopes 1.11, 1.05 and 1.45 imp/s/nA, which are compatible with data from cat literature for the primary range [22,41,42] (Table 9).

3.5. Step current input

The previous test was associated with the steady-state response to an injected step current. The transient response to such an input—the firing rate adaptation—gives a partial picture of the dynamics of each model. Fig. 3 shows the instantaneous firing rate (inverse of the interspike intervals) as a function of time for one of the models. The adaptation follows a time course found in some real MNs (see inset) [37,43].

An alternative view of the adaptation process is based on the comparison of the graphs of (1/1st interspike interval) and (1/steady-state interspike interval) as a function of the current intensity. Such a relation is shown in Fig. 4 (empty circles) for the FF MN model. The effect of the firing rate adaptation is quite clear in the much larger slope of the relation associated with the first interval instantaneous rate when compared with the steady-state relation. The steady-state behavior was quite

Please cite this article as: M.F. Vieira, A.F. Kohn, Compartmental models of mammalian motoneurons of types S, FR and FF and their computer simulation, Comp. Biol. Med. (2006), doi: 10.1016/j.compbiomed.2006.09.001

Table 8
Rheobase

	Type S (nA)	Type FR (nA)	Type FF (nA)
Proposed models	3.02	8.20	19.09
Zengel et al. [24]	5.0 ± 0.3 [2–8]	12.0 ± 0.4 [8–18]	21.3 ± 0.5 [10–38]
Fleshman et al. [55]	5.1 ± 0.5 [2–9]	12.8 ± 0.6 [8–20]	19.7 ± 0.8 [5–27]
Gustaffson and Pinter [40]	[1.2–8.0]	[7.5–15.0]	[14.0–32.0]
Jones and Bawa [2] models	2.53	4.1	–

Table 9
f/I relations slope

	Type S (imp/s/nA)	Type FR (imp/s/nA)	Type FF (imp/s/nA)
Proposed models	1.11	1.05	1.45
Baldissera et al. [22]	–	0.5 and 1.7	0.5 and 1.7
Jones and Bawa [2] models	4.4	5.4	–
Traubs [4,5] models	–	–	2.21

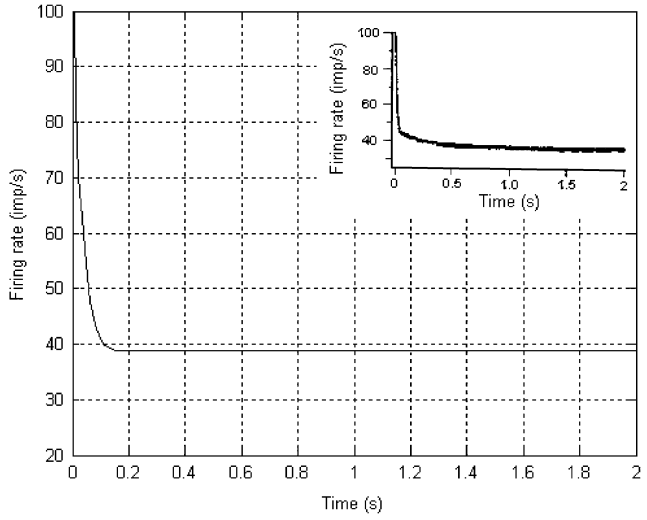

Fig. 3. Instantaneous firing rates for the FR motoneuron model when a 20 nA current step was injected. The points were joined to facilitate the visualization. There is a good agreement with a hypoglossal motoneuron adaptation data shown in the inset (adapted from [43]).

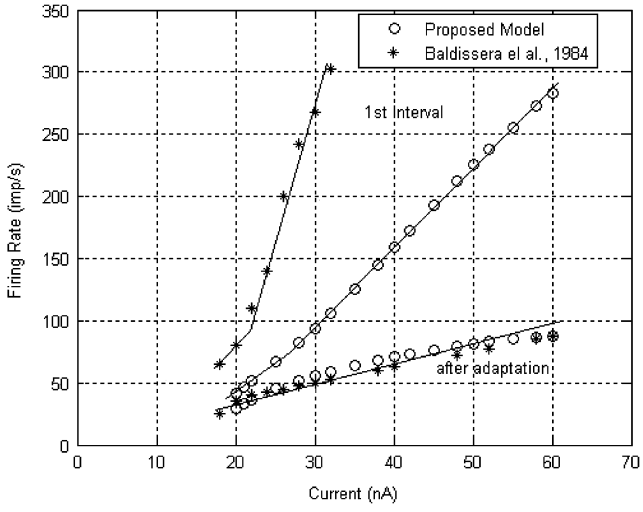

Fig. 4. Graph of f/I data points for the FF motoneuron model (open circles) compared to biological F motoneuron data from Baldissera et al. [22] (asterisks). The steady-state values are practically superimposed. On the other hand, the instantaneous rates corresponding to the first interspike interval are much smaller in the model than in the experimental data. The straight lines are minimum mean square error fits.

similar to that reported for the cat (stars), as reported in [22,38]. On the other hand, there was a larger discrepancy in the first interval relation, the model showing a much smaller slope than that found in the cat data.

A detailed analysis of the somatic currents showed that the type N calcium current decreases after the initial spikes while the type L calcium current increases. This causes a gradual increase in the SK-type potassium current, which has an important influence on the firing rate adaptation in each of the models.

3.6. Ramp current input

The ramp-and-hold currents injected in the somas of the three MN models were similar to those used in cat experiments described in [23,38]. Such inputs are important in testing the dynamics of real and model neurons. As the available experimental data from the literature covers mainly type F MNs, we shall emphasize results for the FF/FR MN models. Fig. 5 shows some results for the FF model, all for ramp-and-hold input currents with a plateau of 38 nA, comparing with the experimental data reported in [22]. In both (a) and (b) in Fig. 5, the first box shows experimental data and the others are from the model simulation. The steady-state discharge rate in all cases was around 70 spikes/s but the transient instantaneous rates show a clear sensitivity to the slope of the input current ramp. Comparing Figs. 5(a) and (b) it can be concluded that the model neuron is able to encode the rate of change of the current. For example, when the slope increased from 0.22 to 1.23 nA/ms, the peak instantaneous firing rate increased from about 80 to

Please cite this article as: M.F. Vieira, A.F. Kohn, Compartmental models of mammalian motoneurons of types S, FR and FF and their computer simulation, Comp. Biol. Med. (2006), doi: 10.1016/j.compbiomed.2006.09.001

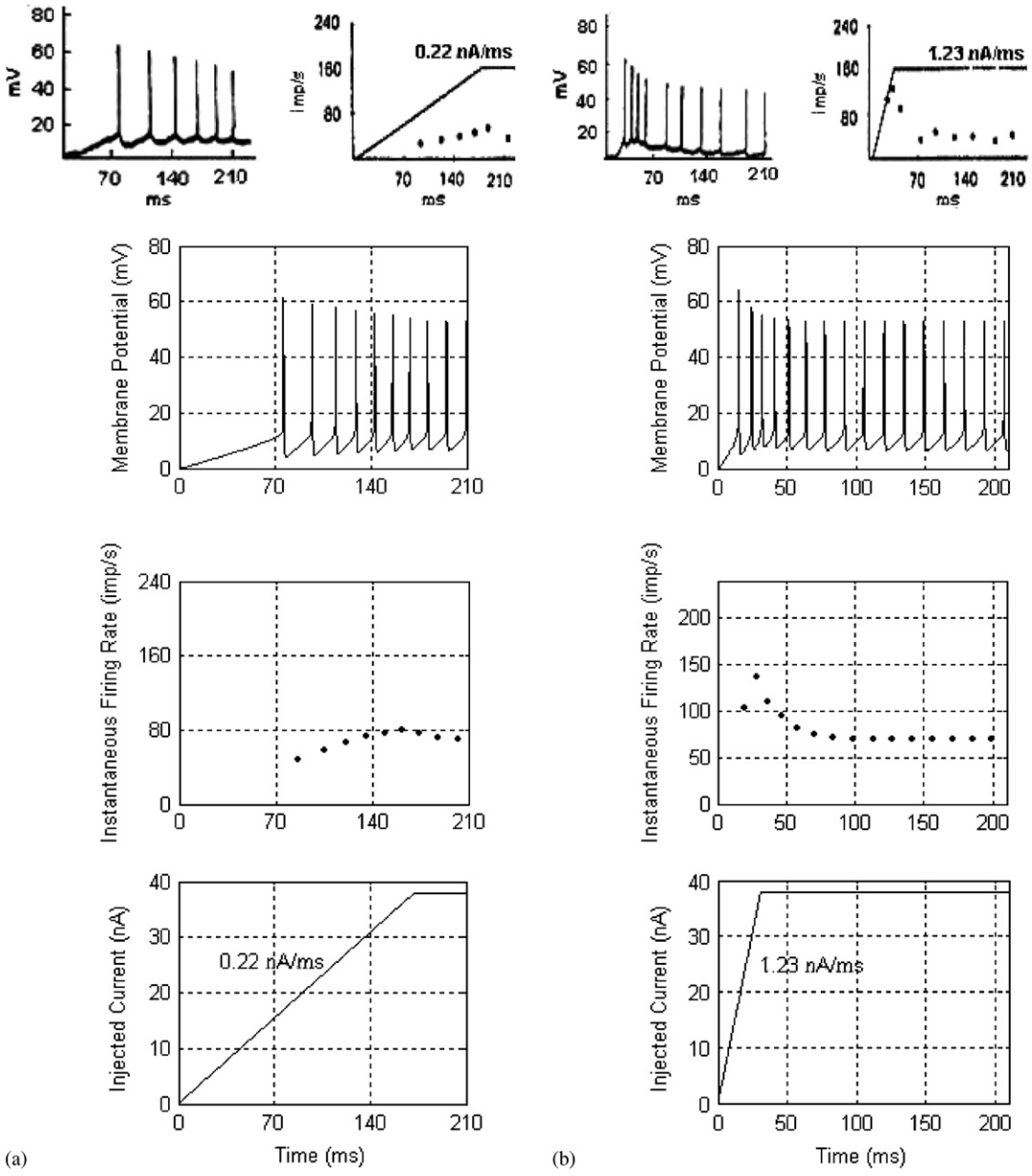

Fig. 5. Plots of the spike trains, instantaneous rates and injected current in the soma for two cases: (a) slope of injected current of 0.22 nA/ms, (b) slope of injected current of 1.23 nA/ms. Both ramp-and-hold input currents had a plateau value 38 nA. The top of each column shows experimental data (spikes at the left and instantaneous rate on the right) adapted from Ref. [22]. The other three graphs in each column refer to results from model simulations.

about 140 spikes/s. These findings are in agreement with experimental data [23,38], if not precisely but in the same order of magnitude. Similar results, except for a smaller steady-state firing rate around 67 spikes/s, were found for the FR model when subjected to the same input currents. When some mathematical models of MNs found in the literature were tested with the ramp-and-hold inputs (or step inputs), their behaviors were quite poor when compared with the experimental results from the literature, probably due to differences in the modeling of the slow dynamic channels in the soma.

A further quantification of the ramp encoding properties of the FF model is shown in Fig. 6, where we plot the instantaneous frequencies for the first to the fourth intervals as a function of the slope of the input current ramp, all for a 38 nA plateau level. The data for the first interval in Fig. 6 is similar to the experimental points obtained in [23] for their Unit 1 (see their Fig. 5C). Also, the increase in the slopes of the relations in Fig. 6 from the first to the fourth intervals reproduces findings from cat MNs [38, their Fig. 3]. The slopes, measured in imp/s/nA/ms, of best line fits to the four plots in their rising phase were 49.4, 81.9, 120.2 and 151.0. In Fig. 7C of [38] a scatterplot is shown relating the slopes for the first interval from 16 type F MNs and the mean of their data is around 60 imp/s/nA/ms, with a range from 43 to 90 imp/s/nA/ms (eliminating an apparent outlier). Therefore, the slope 49.4 imp/s/nA/ms that we found is within the normal range for fast-type MNs.

Please cite this article as: M.F. Vieira, A.F. Kohn, Compartmental models of mammalian motoneurons of types S, FR and FF and their computer simulation, Comp. Biol. Med. (2006), doi: 10.1016/j.compbiomed.2006.09.001

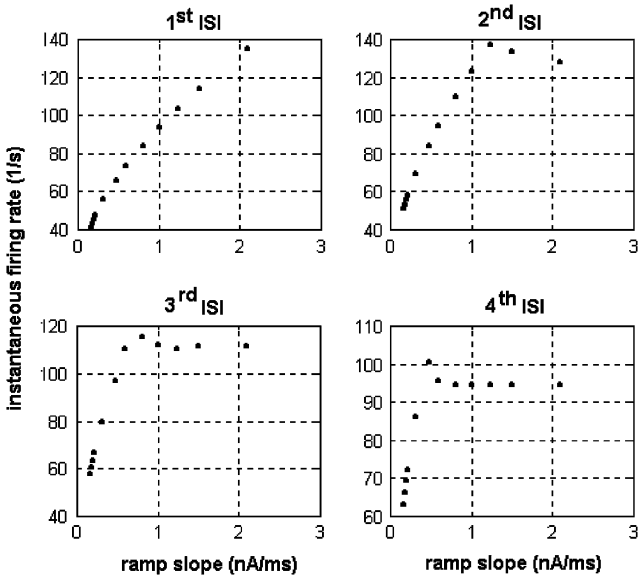

Fig. 6. Relations between MN instantaneous rate and input current ramp slope. The graphs are for the first, second, third and fourth interspike intervals (ISI) obtained from simulations of the FF-type MN model, all for current plateau values 38 nA.

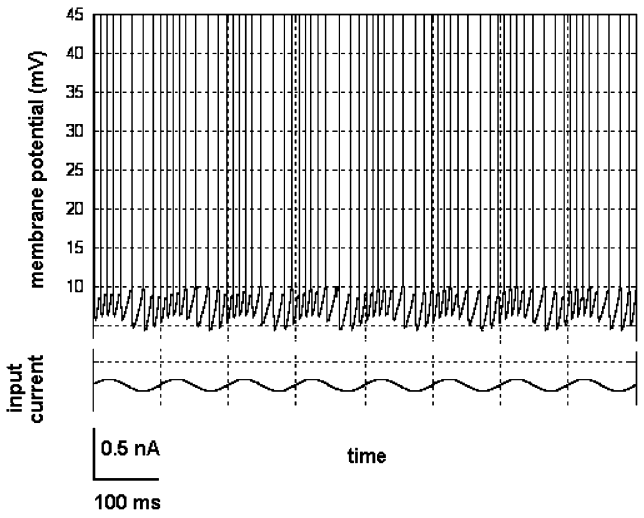

Fig. 7. Membrane potential of the FF MN model showing the resulting spike train for a sinusoidal injected current of 10 Hz. The basal discharge rate of the model was set at 52 spikes/s through the injection of a constant current ($\sim$ 28 nA), upon which the sinusoidal current signal was added.

3.7. Sinusoidal current input

The available experimental data on the frequency response of MNs cover only F-type units [22,39], hence the model validation tests with sinusoidal currents will be useful only for the FR/FF models. A sinusoidal input current at "low" frequencies (e.g., below 10 Hz) caused a reasonably clear frequency modulation of the instantaneous rate of any of the MN models, as exemplified in Fig. 7 for the FF model. Such a sinusoidal input is useful to probe the frequency response function (gain and phase curves) between input current and output firing rate modulation.

The gain and phase curves for the FR and FF models when displayed together with the experimental curves obtained from 10 MNs, based on Table 1 in [22], were contained within the experimental range (not shown). In Fig. 8 we show gain and phase curves for (i) the FF MN model (asterisks), (ii) the model reported in [2,3] (circles), (iii) the model reported in [4] (crosses) and (iv) a fit done in [22] to their cell number 8 (squares, based on their Table 1). This cell was chosen because it had a similar steady-state f/I slope as the FF model (1.45 imp/s/nA, see Results). There is a reasonably good fit of the model's gain curve with the experimental data up to about 12 Hz. The discrepancy for the higher frequencies is possibly due, in part, to the difficulties of fitting a sinusoid to the instantaneous rate modulation. The phase curve for the model follows approximately the average experimental curve albeit with some discrepancies between 1 and 5 Hz. However, the proposed model shows an improvement over the models reported in [2–4] in regard to the frequency response.

3.8. Frequency response between synaptic inputs and somatic current

The somatic current that comes from the dendritic tree is a determinant factor influencing the neuron's firing pattern. In the models, this current is the one being coupled from the first dendritic compartment (dendritic segment d_0) to the soma, which we call I_S. In order to quantify how rhythmic synaptic inputs (which occurs during rhythmic movements) applied at different parts of the dendritic tree affect the soma, we computed the frequency response curves corresponding to synaptic inputs occurring at a few dendritic sites (Fig. 9, for the S-type model). Each synaptic conductance was varied sinusoidally and the amplitude and phase of the resulting fundamental component of the soma current was determined by an FFT. As expected, synaptic inputs nearer the soma resulted in higher cutoff frequencies, as can be seen from Table 1 for the three types of MN models, S, FR and FF. The phase curves for the S-type MN model showed phase shifts around 100° for synapses activated at about 15 Hz farther than the middle of the equivalent dendritic cable. A similar phase shift value occurred for the FR and FF models around 25–30 Hz.

From Table 10 we conclude that the S-type model has lower cutoff frequencies than the type F models, for similarly located synaptic inputs. The FR and FF models showed clearer differences in cutoff frequencies when the synaptic inputs were nearer the soma.

Very similar results were found when the input was a sinusoidal current injected in a given dendritic compartment (instead of sinusoidally varying the conductance), probably because the conductance oscillations were small enough to avoid the influence of neuronal nonlinearities.

3.9. Nonlinearity of the signal transfer from different dendritic sites to the soma

The nonlinear interactions between two dendritic sites, as measured by the somatic current, subjected to independent synaptic inputs may arise both from local effects and from the

Please cite this article as: M.F. Vieira, A.F. Kohn, Compartmental models of mammalian motoneurons of types S, FR and FF and their computer simulation, Comp. Biol. Med. (2006), doi: 10.1016/j.compbiomed.2006.09.001

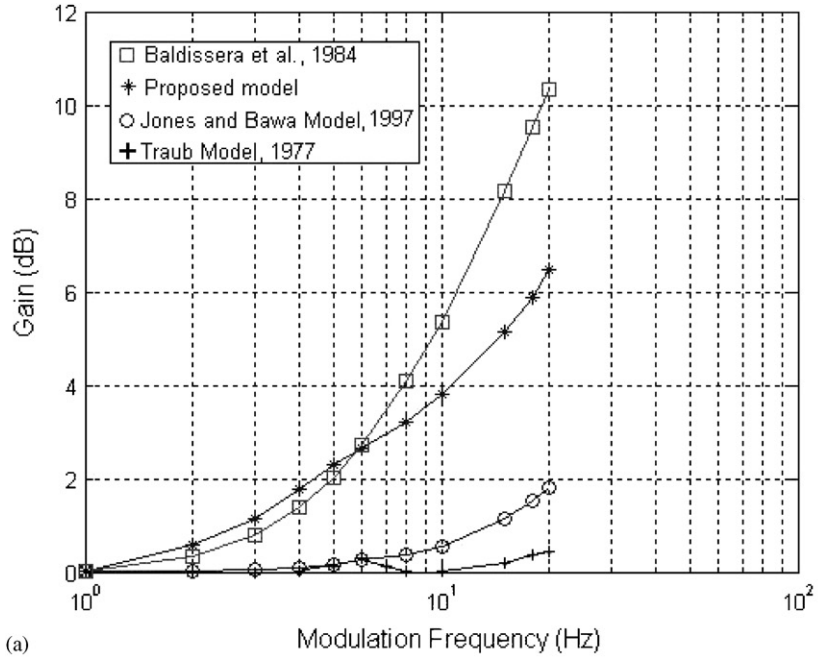

(a)

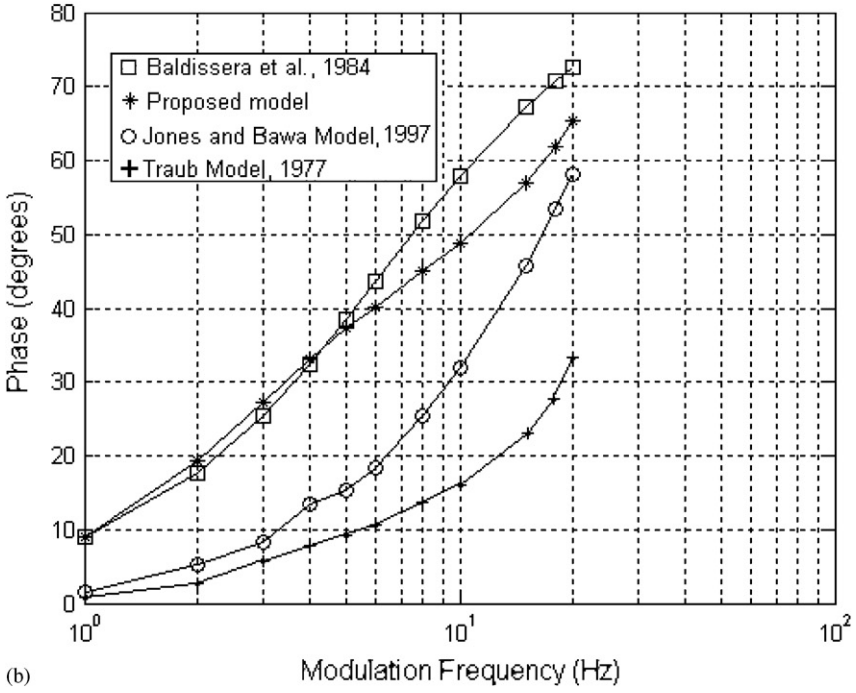

(b)

Fig. 8. Frequency response of the discharge rate modulation obtained from simulations of the FF MN model (asterisks) compared with real MN data (Baldissera et al. [22], open squares), and simulated data from the Jones and Bawa [2] (open circles) and the Traub [4,5] models (crosses). In (a) are the gain curves and in (b) the phase curves.

nonlinear dynamics of the soma. However, if the postsynaptic effects are modeled as changes in dendritic *current* instead of dendritic *conductance*, the local interactions will be linear in the passive dendritic tree model but the soma dynamics may still introduce nonlinearities in the mapping from the synaptic input currents to the current reaching the soma. In these simulations we wanted to study the nonlinearities in the transformation of synaptic inputs to the soma current (which arises from the dendritic segment d_0). A given synaptic input was modeled in two alternate ways: by varying sinusoidally a dendritic compartment *conductance* or by varying its *current*. Two such synaptic inputs were applied to different dendritic compartments, one at a frequency of 7 Hz and the other at 11 Hz. For the comparisons to be valid, the peak-to-peak amplitudes of the currents reaching the soma in the two situations (*conductance* versus *current* dendritic inputs) were made equal. The Fourier transform of the somatic current coming from dendritic segment d_0 was used to determine the harmonic distortions associated with each input

Please cite this article as: M.F. Vieira, A.F. Kohn, Compartmental models of mammalian motoneurons of types S, FR and FF and their computer simulation, Comp. Biol. Med. (2006), doi: 10.1016/j.compbiomed.2006.09.001

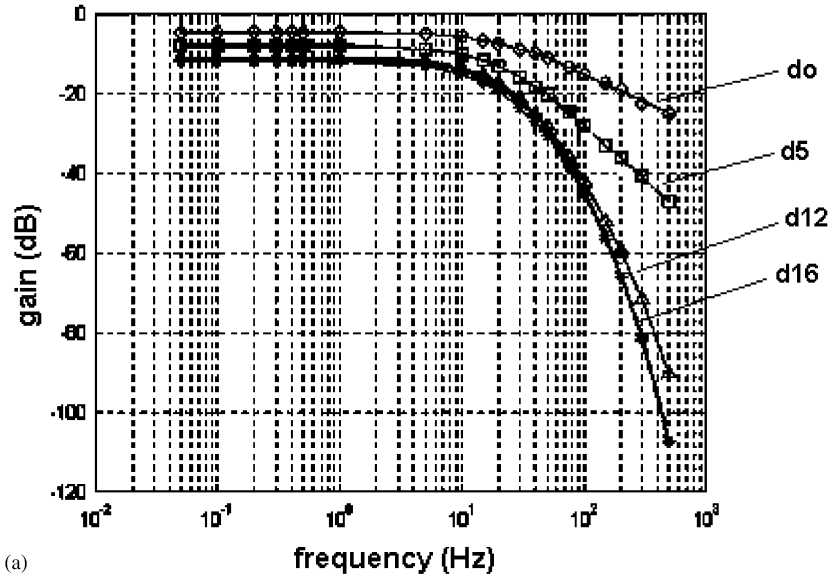

(a)

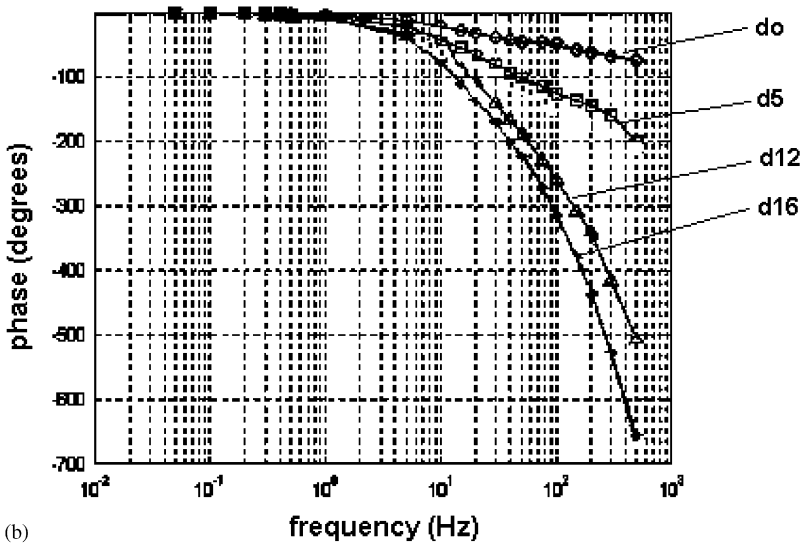

(b)

Fig. 9. Gain (a) and phase curves (b) of the transfer between sinusoidal conductance changes applied at each of the dendritic compartments d_0, d_5, d_{12} and d_{16} and the resulting sinusoidal current entering the soma.

Table 10
Cutoff frequencies between dendritic segments and the soma for S, FR and FF models

	Cutoff frequency at −3 dB (Hz)	Cutoff frequency at −20 dB (Hz)
d_0	25/30/40	500/800/3200
d_5	15/22/22	100/150/200
d_{12}	12/22/20	60/110/110
d_{16}	10/20/14	58/108/90

and the intermodulation distortions caused by the interactions of the two inputs. The former could appear in the spectrum at frequencies such as 14 and 22 Hz, while the latter could appear at spectral frequencies such as 4 and 18 Hz. There are classical quantifiers of system nonlinearity used in electronics as the total harmonic distortion (THD) but we think they are less appropriate in the neurophysiology context. Hence, we chose to quantify the distortions associated with the main spurious components detected in the soma current. More precisely, we measured the ratio of the spectral peaks at each of the main spurious components, found at 4, 14, 18, 22 Hz, to the lowest spectral peak at the two input frequencies (7 or 11 Hz).

Table 11 shows the results obtained from simulations where 11 and 7 Hz sinusoidal synaptic conductance changes were applied to adjacent dendritic segments S_i and S_{i+1}, respectively, to the FF-type MN model (similar conclusions were reached when data from the S and FR models were analyzed). For all dendritic levels, the 7 Hz component had a lower amplitude in the output spectrum than the 11 Hz component, so *it was used as a reference to compute distortion*. The data from Table 11 suggests that the distortion increases as the (conductance changes due to) synaptic inputs occur more distally. Also, the harmonic distortions (i.e., at $2f_2$ and $2f_1$) are smaller than intermodulation distortions when synaptic conductances occur close together (except at the two more distal compartments).

Please cite this article as: M.F. Vieira, A.F. Kohn, Compartmental models of mammalian motoneurons of types S, FR and FF and their computer simulation, Comp. Biol. Med. (2006), doi: 10.1016/j.compbiomed.2006.09.001

Table 11
Levels in dB of the power at each spurious frequency with respect to the power at 7 Hz for the FF model with conductance changes at dendritic segments S_i and S_{i+1}

Dendrites	$f_1 - f_2$ (4.0 Hz)	$2f_2$ (14.0 Hz)	$f_1 + f_2$ (18.0 Hz)	$2f_1$ (22.0 Hz)
0–1	−28.64	−32.75	−29.51	−34.42
2–3	−25.61	−30.56	−26.76	−32.18
4–5	−23.57	−28.73	−24.82	−30.61
6–7	−21.62	−26.55	−22.94	−28.77
8–9	−18.98	−23.98	−20.43	−26.35
10–11	−16.72	−21.72	−18.28	−24.00
12–13	−14.04	−18.37	−15.67	−20.53
14–15	−10.61	−14.66	−12.47	−15.58
16–17	−6.02	−8.71	−8.14	−3.04

Table 12
Levels in dB of the power at each spurious frequency with respect to the power at 7 Hz for the FF model with conductance changes at dendritic segments S_i and S_{i+5}

Dendrites	$f_1 - f_2$ (4.0 Hz)	$2f_2$ (14.0 Hz)	$f_1 + f_2$ (18.0 Hz)	$2f_1$ (22.0 Hz)
0–5	−30.16	−28.35	−31.11	−31.72
2–7	−26.85	−26.17	−27.84	−29.46
4–9	−24.55	−23.46	−25.58	−27.63
6–11	−22.23	−21.06	−23.36	−25.65
8–13	−19.31	−17.71	−20.63	−22.04
10–15	−16.79	−13.75	−18.28	−16.56
12–17	−13.50	−8.16	−15.23	−3.79

The next group of simulations investigated the distortions when the two synaptic inputs, at 11 and 7 Hz, were not on adjacent segments, but were on segments S_i and S_{i+5}, respectively. For all dendritic levels, the 7 Hz component had the lower amplitude in the output spectrum between the 7 and 11 Hz components, so it was used as a reference to compute distortion. The results are shown in Table 12, which shows that again the distortion increases when the inputs occur more distally. Finally, and perhaps surprisingly, if we fix the more proximal synaptic input (e.g., at dendritic segment 4) the *worst-case* distortion level is similar in the situations S_i/S_{i+1}, and S_i/S_{i+5}, but it occurs at different frequencies (4 and 14 Hz, respectively). However, if we take the mean position between the two synaptic locations as being equal in the two situations S_i/S_{i+1}, and S_i/S_{i+5} (e.g., S_i/S_{i+1} at segments 4 and 5 and S_i/S_{i+5} at segments 2 and 7), then the higher distortion occurs when the two synaptic contacts are closer together.

When the two synaptic inputs were simulated by current injection, with the same paradigms as before, the resulting nonlinear effects were quite small, from −52 to −83 dB, being larger for proximal synaptic inputs than for distal, as expected from theoretical considerations.

The results of Sections 3.8 and 3.9 do not have an experimental counterpart, so they should be seen as predictions of what must occur, at least in approximation, with real MNs.

4. Discussion

The modeling effort presented in this paper has two distinguishing features: (a) the three models were developed in an integrated manner and cover the main types of MNs found in vertebrate spinal cords; (b) the model evaluation had a wider scope than found elsewhere, including several dynamic tests of clear functional relevance which are optimally matched to muscle unit behavior [45]. The models exhibited many behaviors found in real MNs and they seem to have a greater level of generalization when compared with other models reported in literature.

In terms of applications of the developed models, the selected level of model complexity makes them well suited to investigations of many single neuron phenomena such as action potential backpropagation on the dendritic tree, spike train variability due to synaptic bombardment on the dendritic tree, effects of synaptic input synchrony on the MN spike train statistics and nonlinear dendritic interactions. We believe the models are also suitable for use in simulators of the behavior of MN pools, if they are implemented in a multiprocessor fast machine or in computer clusters, and use optimized code. Such simulators, if they are required to be reasonably realistic at the neuronal level, have to include MN models that have some representation of the spatio-temporal transformation enacted by dendrites, besides including MN descriptions that cover the gamut from S type to FF type. These aspects were contemplated in the present work.

The dendrite-to-soma synaptic transfer had lowpass characteristics, with cutoff frequencies increasing from the S to the F models and decreasing when the inputs were located more distally. The −3 dB cutoff frequencies were equal or larger than 10 Hz, this lowest value occurring for the most apically located synaptic inputs. In humans the maximum frequencies of

Please cite this article as: M.F. Vieira, A.F. Kohn, Compartmental models of mammalian motoneurons of types S, FR and FF and their computer simulation, Comp. Biol. Med. (2006), doi: 10.1016/j.compbiomed.2006.09.001

rhythmic voluntary muscle activation are usually lower than 10 Hz (unpublished accelerometer measurements obtained in our lab from different human muscles and [39]). Therefore, in terms of such fast rhythmic behaviors, even synaptic inputs occurring at distal parts of the dendritic tree would affect the soma with little attenuation. More complex situations include a possible compensation of the smaller effective length constant [46], when the dendritic tree is under a barrage, with the activation of voltage-dependent dendritic channels turned by neuromodulators [47].

The nonlinear interactions of two independent synaptic inputs occurring at different levels of the dendritic tree were found to be increasing distally when modeled by conductance variations. The nonlinear effects were also higher when the two synaptic inputs were located closer to each other. These results are not a direct consequence of Rall's findings [44,48] because our model includes a strongly nonlinear soma compartment, which could impose a higher nonlinearity for synaptic inputs occurring at proximal dendritic compartments. Actually, if our tests had included higher synaptic conductance variations, proximal synaptic inputs could indeed present stronger nonlinear interactions than inputs located at more intermediate parts of the dendritic tree. The intermodulation nonlinearity, well known to occur in multiplicative interactions between two signals, was higher when the synapses modeled by conductance changes were close together, which would be expected from stronger interactions of the two compartments' membrane potentials. On the other hand, when synaptic inputs were modeled by injecting current in dendritic compartments, the nonlinear effects were very small. These effects decreased when the synapses moved distally, as they became more isolated from the nonlinear somatic conductances. The frequency domain analysis we adopted to quantify nonlinear dendritic effects is a novel feature of this work. When compared with some other approaches (e.g., that quantify the summation of current reaching the soma), it has the advantage of including the *dynamics* of the soma and the dendritic tree. The sinusoidal variation of conductance applied to a given dendritic compartment could represent what happens during rhythmic movements. In such conditions, the MNs will be receiving multiple synaptic activations from descending pathways exhibiting a periodic variation in the intensity of (the point processes associated with) the spike trains. The nonlinearities uncovered by the computer simulations were usually quite small, with the exception of synaptic inputs located at the very distal dendritic compartments.

From the available anatomical data it is not clear at the moment if there are specific pathways that synapse only at the most distal dendritic portions [49]. However, the dendritic tree may be switched (e.g., by serotonin released from the brainstem) from passive dynamics (i.e., with fixed conductances), modeled in the present work, to an active one, with voltage-sensitive conductances [50]. Very probably, the ensuing nonlinearities in the mapping of rhythmic synaptic activations to somatic current (e.g., evaluated with the method proposed in the present work) will be much greater than that for the passive dendritic case. The functional consequences could permeate to the study of neurological diseases [51].

The model fitting was done with the human modeler always in the feedback loop. There was an ad hoc search of the most important parameters for a given target response feature or behavior (see Section 2.1.11). In a restricted sense, an empirical sensitivity analysis was realized for a subset of the model parameters. However, it would certainly be a challenging and fruitful effort to apply more formal computer-based approaches to neuronal model fitting [52–54] in future work on mammalian MN modeling.

In conclusion, three models for cat MNs were developed that tried to represent some of the main known biophysical ionic channels and some basic dendritic structure. The models were able to mimic several dynamic behaviors found in real MNs. The frequency responses associated with synaptic inputs occurring at different dendritic levels suggested that even distal synaptic inputs may drive the MN at the maximum frequency found in physiological oscillatory movement. Both harmonic and intermodulation distortions were found when two synaptic inputs activated different dendritic regions.

5. Summary

Mathematical models of MNs of the three main types—S, FR and FF—were developed based on cat MN data. The models, represented by sets of nonlinear differential equations, were encoded in C++. Each of the three models was composed of three main compartments: initial segment, soma and dendritic tree. The initial segment was described by a Hodgkin–Huxley-type model. The soma included a description of slow potassium currents, calcium currents and a calcium-dependent slow potassium current. The dendritic tree was modeled as a series association of passive equivalent cylinders of varying diameters. The parameters were based on cat MN morphological and electrical data. The dynamics of the channels associated with the somatic currents gave the models the capability of reproducing important physiological features such as AHP summation and MN firing adaptation. The models also reproduced the sensitivity of real MNs to ramp and sinusoidal currents injected in the soma. In particular, the models showed increased instantaneous firing rates to faster ramp inputs and to higher frequencies of sinusoidal inputs.

Other computer simulations reported here include the analysis of the frequency response of the somatic current with respect to synaptic inputs applied at different levels of the dendritic tree of each model. The resulting frequency responses were of the lowpass type, with 10 Hz being the smallest cutoff frequency found for synaptic conductance modulations occurring at the most apical dendritic compartment of the type S MN model. Finally, nonlinear interactions between sinusoidally varying dendritic conductances occurring at two compartments, as measured from the current reaching the soma, were found to be higher for more distal compartments. The resulting models should be useful in computer simulation studies of the dynamics of single motor units in isolation or as parts of a large-scale neuronal network representing the circuitry of the spinal cord.

Please cite this article as: M.F. Vieira, A.F. Kohn, Compartmental models of mammalian motoneurons of types S, FR and FF and their computer simulation, Comp. Biol. Med. (2006), doi: 10.1016/j.compbiomed.2006.09.001

Appendix

Membrane conductances and capacitances of the dendritic compartments for the three MN models:

Dendritic compartments	For type S MN model		For type FR MN model		For type FF MN model	
	g_{d_i} (mS)	C_{d_i} (μF)	g_{d_i} (mS)	C_{d_i} (μF)	g_{d_i} (mS)	C_{d_i} (μF)
d_0	1.96×10^{-5}	3.93×10^{-4}	5.72×10^{-5}	6.28×10^{-4}	2.75×10^{-5}	5.50×10^{-4}
d_1	1.96×10^{-5}	3.93×10^{-4}	5.72×10^{-5}	6.28×10^{-4}	2.75×10^{-5}	5.50×10^{-4}
d_2	1.96×10^{-5}	3.93×10^{-4}	5.72×10^{-5}	6.28×10^{-4}	2.75×10^{-5}	5.50×10^{-4}
d_3	1.96×10^{-5}	3.93×10^{-4}	5.72×10^{-5}	6.28×10^{-4}	2.75×10^{-5}	5.50×10^{-4}
d_4	1.96×10^{-5}	3.93×10^{-4}	5.57×10^{-5}	6.13×10^{-4}	2.75×10^{-5}	5.50×10^{-4}
d_5	1.96×10^{-5}	3.93×10^{-4}	5.43×10^{-5}	5.97×10^{-4}	2.59×10^{-5}	5.18×10^{-4}
d_6	1.92×10^{-5}	3.83×10^{-4}	4.86×10^{-5}	5.34×10^{-4}	2.36×10^{-5}	4.71×10^{-4}
d_7	1.67×10^{-5}	3.34×10^{-4}	4.29×10^{-5}	4.71×10^{-4}	2.11×10^{-5}	4.23×10^{-4}
d_8	1.47×10^{-5}	2.95×10^{-4}	3.72×10^{-5}	4.08×10^{-4}	1.77×10^{-5}	3.53×10^{-4}
d_9	1.28×10^{-5}	2.55×10^{-4}	1.57×10^{-5}	1.73×10^{-4}	7.62×10^{-6}	1.52×10^{-4}
d_{10}	9.82×10^{-6}	1.96×10^{-4}	1.29×10^{-5}	1.41×10^{-4}	6.28×10^{-6}	1.26×10^{-4}
d_{11}	7.85×10^{-6}	1.57×10^{-4}	1.14×10^{-5}	1.26×10^{-4}	5.30×10^{-6}	1.06×10^{-4}
d_{12}	2.95×10^{-6}	5.89×10^{-5}	1.00×10^{-5}	1.10×10^{-4}	4.32×10^{-6}	8.64×10^{-5}
d_{13}	2.06×10^{-6}	4.12×10^{-5}	8.29×10^{-6}	9.11×10^{-5}	3.53×10^{-6}	7.07×10^{-5}
d_{14}	1.28×10^{-6}	2.55×10^{-5}	6.43×10^{-6}	7.07×10^{-5}	2.95×10^{-6}	5.89×10^{-5}
d_{15}	3.68×10^{-7}	7.36×10^{-6}	5.00×10^{-6}	5.50×10^{-5}	1.94×10^{-6}	3.89×10^{-5}
d_{16}	1.23×10^{-7}	2.46×10^{-6}	2.29×10^{-6}	2.51×10^{-5}	1.10×10^{-6}	2.20×10^{-5}
d_{17}	–	–	7.15×10^{-7}	7.85×10^{-6}	2.95×10^{-7}	5.89×10^{-6}
d_{18}	–	–	2.87×10^{-7}	3.15×10^{-6}	7.90×10^{-8}	1.57×10^{-6}

Coupling conductances between adjacent compartments:

	For type S MN model (mS)	For type FR MN model (mS)	For type FF MN model (mS)
$g_{S,\mathrm{IS}}$	1.53×10^{-3}	2.12×10^{-3}	2.13×10^{-3}
g_{S,d_0}	5.10×10^{-3}	6.65×10^{-3}	5.15×10^{-3}
g_{d_0,d_1}	1.40×10^{-3}	3.59×10^{-3}	2.75×10^{-3}
g_{d_1,d_2}	1.40×10^{-3}	3.59×10^{-3}	2.75×10^{-3}
g_{d_2,d_3}	1.40×10^{-3}	3.59×10^{-3}	2.75×10^{-3}
g_{d_3,d_4}	1.40×10^{-3}	3.50×10^{-3}	2.75×10^{-3}
g_{d_4,d_5}	1.40×10^{-3}	3.32×10^{-3}	2.59×10^{-3}
g_{d_5,d_6}	1.37×10^{-3}	2.88×10^{-3}	2.21×10^{-3}
g_{d_6,d_7}	1.15×10^{-3}	2.27×10^{-3}	1.80×10^{-3}
g_{d_7,d_8}	8.87×10^{-4}	1.73×10^{-3}	1.34×10^{-3}
g_{d_8,d_9}	6.77×10^{-4}	1.79×10^{-3}	1.36×10^{-3}
$g_{d_9,d_{10}}$	4.41×10^{-4}	1.74×10^{-3}	1.38×10^{-3}
$g_{d_{10},d_{11}}$	2.74×10^{-4}	1.28×10^{-3}	9.56×10^{-4}
$g_{d_{11},d_{12}}$	2.38×10^{-4}	9.96×10^{-4}	6.53×10^{-4}
$g_{d_{12},d_{13}}$	1.66×10^{-4}	7.16×10^{-4}	4.36×10^{-4}
$g_{d_{13},d_{14}}$	6.85×10^{-5}	7.27×10^{-4}	2.98×10^{-4}
$g_{d_{14},d_{15}}$	3.79×10^{-5}	2.74×10^{-4}	1.89×10^{-4}
$g_{d_{15},d_{16}}$	6.31×10^{-6}	1.27×10^{-4}	9.44×10^{-5}
$g_{d_{16},d_{17}}$	–	5.10×10^{-5}	3.12×10^{-5}
$g_{d_{17},d_{18}}$	–	1.70×10^{-5}	4.93×10^{-6}

Please cite this article as: M.F. Vieira, A.F. Kohn, Compartmental models of mammalian motoneurons of types S, FR and FF and their computer simulation, Comp. Biol. Med. (2006), doi: 10.1016/j.compbiomed.2006.09.001

Soma currents:

		For type S MN model (mS)	For type FR MN model (mS)	For type FF MN model (mS)
Sodium current	$I_{Na(soma)} = g_{max} m^3 h (V_m - E_{Na})$	$g_{max} = 140\,mS/cm^2$	$g_{max} = 140\,mS/cm^2$	$g_{max} = 140\,mS/cm^2$
		$\alpha_m = \frac{7+(-0.4*V_m)}{e^{((V_m-17.5)/-5)}-1}$	$\alpha_m = \frac{7+(-0.4*V_m)_{-3}}{e^{((V_m-17.5)/-5)}-1}$	$\alpha_m = \frac{7+(-0.4*V_m)}{e^{((V_m-17.5)/-5)}-1}$
	$E_{Na} = 115\,mV$	$\beta_m = \frac{(0.4*V_m)-18}{e^{((V_m-45)/5)}-1}$	$\beta_m = \frac{(0.4*V_m)-18}{e^{((V_m-45)/5)}-1}$	$\beta_m = \frac{(0.4*V_m)-18}{e^{((V_m-45)/5)}-1}$
		$\alpha_h = \frac{0.15}{e^{((V_m-34.26)/18.19)}}$	$\alpha_h = \frac{0.15}{e^{((V_m-34.26)/18.19)}}$	$\alpha_h = \frac{0.15}{e^{((V_m-34.26)/18.19)}}$
		$\beta_h = \frac{4}{e^{((V_m-40)/-10)}+1}$	$\beta_h = \frac{4}{e^{((V_m-40)/-10)}+1}$	$\beta_h = \frac{4}{e^{((V_m-40)/-10)}+1}$
Fast potassium current	$I_{Kf(soma)} = g_{max} n^4 (V_m - E_K)$	$g_{max} = 35\,mS/cm^2$	$g_{max} = 35\,mS/cm^2$	$g_{max} = 35\,mS/cm^2$
	$E_K = -10\,mV$	$\alpha_n = \frac{0.4+(-0.02*V_m)}{e^{((V_m-20)/-10)}-1}$	$\alpha_n = \frac{0.4+(-0.02*V_m)}{e^{((V_m-20)/-10)}-1}$	$\alpha_n = \frac{0.4+(-0.02*V_m)}{e^{((V_m-20)/-10)}-1}$
		$\beta_n = \frac{0.16}{e^{((V_m-33.79)/66.56)}-0.032}$	$\beta_n = \frac{0.16}{e^{((V_m-33.79)/66.56)}-0.032}$	$\beta_n = \frac{0.16}{e^{((V_m-33.79)/66.56)}-0.032}$
Slow potassium current type BK	$I_{BKs(soma)} = g_{max} q^2 r (V_m - E_K)$	$g_{max} = 6.8\,mS/cm^2$	$g_{max} = 35\,mS/cm^2$	$g_{max} = 32\,mS/cm^2$
	$E_K = -10\,mV$	$\alpha_q = \frac{3.5}{e^{((V_m-45)/-4)}+1}$	$\alpha_q = \frac{3.5}{e^{((V_m-45)/-4)}+1}$	$\alpha_q = \frac{3.5}{e^{((V_m-45)/-4)}+1}$
		$\beta_q = \frac{0.018}{e^{((V_m+50)/-0.001)}+1}$	$\beta_q = \frac{0.042}{e^{((V_m+50)/-0.001)}+1}$	$\beta_q = \frac{0.048}{e^{((V_m+50)/-0.001)}+1}$
		$r = \frac{[Ca^{2+}]}{[Ca^{2+}]+0.4}$	$r = \frac{[Ca^{2+}]}{[Ca^{2+}]+0.4}$	$r = \frac{[Ca^{2+}]}{[Ca^{2+}]+0.2}$
Slow potassium current type SK	$I_{SKs(soma)} = g_{max}([Ca^{2+}]/K_d)^2 (V_m - E_K)$	$g_{max} = 0.3\,mS/cm^2$	$g_{max} = 23.4\,mS/cm^2$	$g_{max} = 22\,mS/cm^2$
	$E_K = -10\,mV$	$K_d = 0.04$	$K_d = 0.5$	$K_d = 0.8$
Calcium	$I_{CaN} = g_{max} m_N^2 h_N (V_m - E_{Ca})$	$g_{max} = 1.4\,mS/cm^2$	$g_{max} = 2.13\,mS/cm^2$	$g_{max} = 2.0\,mS/cm^2$
Current type N		$m_{N\,inf} = \frac{1}{1+e^{((V_m-40)/-5)}}$	$m_{N\,inf} = \frac{1}{1+e^{((V_m-40)/-5)}}$	$m_{N\,inf} = \frac{1}{1+e^{((V_m-40)/-5)}}$
		$\tau_{m_N} = 4$	$\tau_{m_N} = 4$	$\tau_{m_N} = 4$
		$m_{N\,inf} = \frac{1}{1+e^{((V_m-25)/10)}}$	$m_{N\,inf} = \frac{1}{1+e^{((V_m-25)/10)}}$	$m_{N\,inf} = \frac{1}{1+e^{((V_m-25)/10)}}$
		$\tau_{h_N} = 40$	$\tau_{h_N} = 40$	$\tau_{h_N} = 40$
Calcium current type L	$I_{CaL} = g_{max} m_L^2 (V_m - E_{Ca})$	$g_{max} = 1.8\,mS/cm^2$	$g_{max} = 2.7\,mS/cm^2$	$g_{max} = 2.5\,mS/cm^2$
	$E_{Ca} = 140\,mV$	$m_{L\,inf} = \frac{1}{1+e^{((V_m-25)/-5)}}$	$m_{L\,inf} = \frac{1}{1+e^{((V_m-25)/-5)}}$	$m_{L\,inf} = \frac{1}{1+e^{((V_m-25)/-5)}}$
		$\tau_{m_N} = 60$	$\tau_{m_N} = 60$	$\tau_{m_N} = 60$

Initial segment currents:

		For type S MN model	For type FR MN model	For type FF MN model
Sodium current	$I_{Na(IS)} = g_{max} m^3 h (V_m - E_{Na})$	$g_{max} = 500\,mS/cm^2$	$g_{max} = 500\,mS/cm^2$	$g_{max} = 500\,mS/cm^2$
	$E_{Na} = 115\,mV$	$\alpha_m = \frac{4+(-0.4*V_m)}{e^{((V_m-10)/-5)}-1}$	$\alpha_m = \frac{4+(-0.4*V_m)_{-3}}{e^{((V_m-10)/-5)}-1}$	$\alpha_m = \frac{4+(-0.4*V_m)}{e^{((V_m-10)/-5)}-1}$
		$\beta_m = \frac{(0.4*V_m)-14}{e^{((V_m-35)/5)}-1}$	$\beta_m = \frac{(0.4*V_m)-14}{e^{((V_m-35)/5)}-1}$	$\beta_m = \frac{(0.4*V_m)-14}{e^{((V_m-35)/5)}-1}$
		$\alpha_h = \frac{0.16}{e^{((V_m-37.78)/18.14)}}$	$\alpha_h = \frac{0.16}{e^{((V_m-37.78)/18.14)}}$	$\alpha_h = \frac{0.16}{e^{((V_m-37.78)/18.14)}}$
		$\beta_h = \frac{4}{e^{((V_m-30)/-10)}+1}$	$\beta_h = \frac{4}{e^{((V_m-30)/-10)}+1}$	$\beta_h = \frac{4}{e^{((V_m-30)/-10)}+1}$
Fast potassium current	$I_{Kf(IS)} = g_{max} n^4 (V_m - E_K)$	$g_{max} = 100\,mS/cm^2$	$g_{max} = 100\,mS/cm^2$	$g_{max} = 100\,mS/cm^2$
	$E_K = -10\,mV$	$\alpha_n = \frac{0.2+(-0.02*V_m)}{e^{((V_m-10)/-10)}-1}$	$\alpha_n = \frac{0.2+(-0.02*V_m)}{e^{((V_m-10)/-10)}-1}$	$\alpha_n = \frac{0.2+(-0.02*V_m)}{e^{((V_m-10)/-10)}-1}$
		$\beta_n = \frac{0.15}{e^{((V_m-33.79)/71.86)}-0.01}$	$\beta_n = \frac{0.15}{e^{((V_m-33.79)/71.86)}-0.01}$	$\beta_n = \frac{0.15}{e^{((V_m-33.79)/71.86)}-0.01}$

Please cite this article as: M.F. Vieira, A.F. Kohn, Compartmental models of mammalian motoneurons of types S, FR and FF and their computer simulation, Comp. Biol. Med. (2006), doi: 10.1016/j.compbiomed.2006.09.001

Synaptic currents:

$I_{\text{syn}}(t) = g_{\text{syn}}(t) * (V_m - E_{\text{syn}})$,

where $g_{\text{syn}} = g_{\max} t^{\alpha} e^{-\alpha t/\tau}$, $\alpha = 1$, $\tau = 0.2\,\text{ms}$, $E_{\text{syn}} = 70\,\text{mV}$.

References

[1] W. Rall, Branching dendritic trees and motoneuron membrane resistivity, Exp. Neurol. 1 (1959) 491–527.
[2] K.E. Jones, P. Bawa, Computer simulation of the responses of human motoneurons to composite Ia EPSPs: effects of background firing rate, J. Neurophysiol. 77 (1997) 405–420.
[3] K.E. Jones, P. Bawa, A comparison of human motoneuron data to simulated data using cat motoneuron models, J. Physiol.—Paris 93 (1999) 43–59.
[4] R.D. Traub, Motorneurons of different geometry and the size principle, Biol. Cybern. 25 (1977) 163–176.
[5] R.D. Traub, R. Llinás, The spatial distribution of ionic conductances in normal and axotomized motoneurons, Neuroscience 2 (1977) 829–849.
[6] Y. Dai, K.E. Jones, B. Fedirchuk, D.A. McCrea, L.M. Jordan, A modelling study of locomotion-induced hyperpolarization of voltage threshold in cat lumbar motoneurons, J. Physiol. 544 (2) (2002) 521–536.
[7] C.C. McIntyre, W.M. Grill, Extracellular stimulation of central neurons: influence of stimulus waveform and frequency on neuronal output, J. Neurophysiol. 88 (2002) 1592–1604.
[8] S. Cushing, T. Bui, P.K. Rose, Effect of nonlinear summation of synaptic currents on the input–output properties of spinal motoneurons, J. Neurophysiol. 94 (2005) 3465–3478.
[9] F. Baldissera, B. Gustafsson, Afterhyperpolarization conductance time course in lumbar motoneurons of cat, Acta Physiol. Scand. 91 (1974) 512–527.
[10] F. Baldissera, B. Gustafsson, Firing behaviour of a neuron model based on the afterhyperpolarization conductance time course. First interval firing, Acta Physiol. Scand. 91 (1974) 528–544.
[11] F. Baldissera, B. Gustafsson, Firing behaviour of a neuron model based on the afterhyperpolarization conductance time course and algebraical summation. Adaptation and steady state firing, Acta Physiol. Scand. 92 (1974) 27–47.
[12] R.K. Powers, A variable-threshold motoneuron model that incorporates time and voltage-dependent potassium and calcium conductances, J. Neurophysiol. 70 (1993) 246–262.
[13] V. Booth, J. Rinzel, O. Kiehn, Compartmental model of vertebrate motoneurons for Ca^{++} dependent spiking and plateau potentials under pharmacological treatment, J. Neurophysiol. 78 (1997) 3371–3385.
[14] C. Capaday, A re-examination of the possibility of controlling the firing rate gain of neurons by balancing excitatory and inhibitory conductances, Exp. Brain Res. 143 (2002) 67–77.
[15] O. Ekeberg, P. Wallen, A. Lansner, H. Traven, L. Brodin, S. Grillner, A computer-based model for realistic simulations of neural networks. 1. The single neuron and synaptic interaction, Biol. Cybern. 65 (1991) 81–90.
[16] C.J. Heckman, M.D. Binder, Computer simulation of the steady-state input–output function of the cat medial gastrocnemius motoneuron pool, J. Neurophysiol. 65 (1991) 952–967.
[17] P.J. Slot, T. Sinkjaer, Simulations of the alpha motoneuron pool electromyogram reflex at different preactivation levels in man, Biol. Cybern. 70 (1994) 351–358.
[18] M.G. Maltenfort, C.J. Heckman, W.Z. Rymer, Decorrelating actions of Renshaw interneurons on the firing of spinal motoneurons within a motor nucleus: a simulation study, J. Neurophysiol. 80 (1998) 309–323.
[19] R.M. Nussbaumer, D.G. Ruegg, L.M. Studer, J.P. Gabriel, Computer simulation of the motoneuron pool–muscle complex. I. Input system and motoneuron pool, Biol. Cybern. 86 (2002) 317–333.
[20] R. Cisi, A.F. Kohn, Spinal cord neuronal network simulator, in: Conference of the Canadian Medical and Biological Engineering Society, Que., Canada, 2004.
[21] R.E. Burke, The spinal cord: ventral horn, in: G.M. Shepherd (Ed.), Synaptic Organization of the Brain, Oxford University Press, New York, 2003.
[22] F. Baldissera, P. Campadelli, L. Piccinelli, The dynamic response of cat alpha-motoneurons investigated by intracellular injection of sinusoidal currents, Exp. Brain Res. 54 (1984) 275–282.
[23] F. Baldissera, P. Campadelli, L. Piccinelli, The dynamic response of cat gastrocnemius motor units investigated by ramp-current injection into their motoneurons, J. Physiol. 387 (1987) 317–330.
[24] J.E. Zengel, S.A. Reid, G.W. Sypert, J.B. Munson, Membrane electrical-properties and prediction of motor-unit type of medial gastrocnemius motoneurons in the cat, J. Neurophysiol. 53 (1985) 1323–1344.
[25] D. Kernell, The limits of firing frequency in cat lumbosacral motoneurons possessing different time course of afterhyperpolarization, Acta Physiol. Scand. 65 (1965) 87–100.
[26] D. Kernell, R. Bakels, J.C.V.M. Copray, Discharge properties of motoneurons: how are they matched to the properties and use of their muscle units?, J. Physiol.—Paris 93 (1999) 87–96.
[27] M.D. Binder, C.J. Heckman, R.K. Powers, The physiological control of motoneuron activity, in: L.B. Rowell, J.T. Shepherd (Eds.), Handbook of Physiology, section 12, Oxford University Press, New York, 1996.
[28] S. Cullheim, J.W. Fleshman, L.L. Glenn, R.E. Burke, Membrane area and dendritic structure in type-identified triceps surae alpha motoneurons, J. Comp. Neurol. 255 (1987) 68–81.
[29] J.W. Fleshman, I. Segev, R.E. Burke, Electrotonic architecture of type-identified alpha-motoneurons in the cat spinal cord, J. Neurophysiol. 60 (1988) 60–85.
[30] J.G. McLarnon, Potassium currents in motoneurons, Prog. Neurobiol. 47 (1995) 513–531.
[31] D.G. Goroso, R.R.L. Cisi, A.F. Kohn, The amplitude and phase responses of the firing rates of some motoneuron models, BioSystems 58 (2000) 33–39.
[32] I. Aradi, W.R. Holmes, Role of multiple calcium and calcium-dependent conductances in regulation of hippocampal dentate granule cell excitability, J. Comput. Neurosci. 6 (1999) 215–235.
[33] M.D. Binder, C.J. Heckman, R.K. Powers, The physiological control of motoneuron activity, in: L.B. Rowell, J.T. Shepherd (Eds.), Handbook of Physiology. Section 12: Exercise: Regulation and Integration of Multiple Systems, Oxford University Press, New York, 1996.
[34] C.G. Kukulka, P. Clamann, Comparison of the recruitment and discharge properties of motor units in human brachial biceps and adductor pollicis during isometric contractions, Brain Res. 219 (1981) 45–55.
[35] C.J. De Luca, P.J. Foley, Z. Erim, Motor unit properties in constant-force isometric contractions, J. Neurophysiol. 76 (1996) 1503–1516.
[36] D. Kernell, High-frequency repetitive firing of cat lumbosacral motoneurons stimulated by long-lasting injected currents, Acta Physiol. Scand. 65 (1965) 74–86.
[37] P.C. Schwindt, W.E. Crill, Membrane properties of cat spinal motoneurons, in: R.A. Davidoff (Ed.), Handbook of the Spinal Cord, Marcel Dekker, New York, 1984.
[38] F. Baldissera, P. Campadelli, L. Piccinelli, Neural encoding of input transients investigated by intracellular injection of ramp currents in cat alpha-motoneurons, J. Physiol. 328 (1982) 73–86.
[39] F. Baldissera, P. Cavallari, G. Cerri, Motoneuronal pre-compensation for the low-pass filter characteristics of muscle. A quantitative appraisal in cat muscle units, J. Physiol. 511 (1998) 611–627.
[40] B. Gustaffson, M.J. Pinter, An investigation of threshold properties among cat spinal alfa-motoneurons, J. Physiol. 357 (1984) 453–483.
[41] D. Kernell, Rhythmic properties of motoneurons innervating muscle fibres of different speed in m. gastrocnemius medialis of the cat, Brain Res. 160 (1979) 159–162.
[42] P.C. Schwindt, W.H. Calvin, Membrane-potential trajectories between spikes underlying motoneuron firing rates, J. Neurophysiol. 35 (1972) 311–325.
[43] A. Sawczuk, R.K. Powers, M.D. Binder, Contribution of outward currents to spike-frequency adaptation in hypoglossal motoneurons of the rat, J. Neurophysiol. 78 (1997) 2246–2253.

Please cite this article as: M.F. Vieira, A.F. Kohn, Compartmental models of mammalian motoneurons of types S, FR and FF and their computer simulation, Comp. Biol. Med. (2006), doi: 10.1016/j.compbiomed.2006.09.001

[44] W. Rall, Theoretical significance of dendritic trees for neuronal input–output relations, in: R.F. Reiss (Ed.), Neural Theory and Modeling, Stanford University Press, Palo Alto, 1964.
[45] A.F. Kohn, M.F. Vieira, Optimality in the encoding/decoding relations of motoneurons and muscle units, BioSystems 67 (2002) 113–119.
[46] C. Koch, Biophysics of Computation, Oxford University Press, New York, 1999.
[47] E.P. Cook, D. Johnston, Voltage-dependent properties of dendrites that eliminate location-dependent variability of synaptic input, J. Neurophysiol. 81 (1999) 535–543.
[48] W. Rall, Distinguishing theoretical synaptic potentials computed for different soma-dendritic distributions of synaptic input, J. Neurophysiol. 30 (1967) 1138–1168.
[49] R.E. Fyffe, Spinal motoneurons: synaptic inputs and receptor organization, in: T.C. Cope (Ed.), Motor Neurobiology of the Spinal Cord, CRC Press, Boca Raton, FL, 2001.
[50] C.J. Heckman, R.H. Lee, R.M. Brownstone, Hyperexcitable dendrites in motoneurons and their neuromodulatory control during motor behavior, Trends Neurosci. 26 (2003) 688–695.
[51] M.A. Gorassini, M.E. Knash, P.J. Harvey, D.J. Bennett, J.F. Yang, Role of motoneurons in the generation of muscle spasms after spinal cord injury, Brain 127 (2004) 2247–2258.
[52] O. David, S.J. Kiebel, L.M. Harrison, J. Mattout, J.M. Kilner, K.J. Friston, Dynamic causal modeling of evoked responses in EEG and MEG, NeuroImage 30 (2006) 1255–1272.
[53] K. Bush, J. Knight, C. Anderson, Optimizing conductance parameters of cortical neural models via electrotonic partitions, Neural Networks 18 (2005) 488–496.
[54] M.C. Vanier, J.M. Bower, A comparative survey of automated parameter-search methods for compartmental neural models, J. Comput. Neurosci. 7 (1999) 149–171.
[55] J.W. Fleshman, J.B. Munson, G.W. Sypert, W.A. Friedman, Rheobase, input resistance, and motor-unit type in medial gastrocnemius motoneurons in the cat, J. Neurophysiol. 46 (1981) 1326–1338.

Marcus F. Vieira received his B.S.E.E. from the Federal University of Goiás and his M.S.E.E. and Ph.D. from the University of São Paulo, Brazil. He also holds a B.S. in physical education from the Federal University of Goiás, where he is now an Adjunt Professor and directs the Laboratory of Biomechanics. His current research is in computational neuroscience, biomechanics and human motor control.

André F. Kohn received the B.S.E.E. and M.S.E.E. degrees from the University of São Paulo, Brazil, and the Ph.D. from the University of California at Los Angeles, USA. He has done research at the National Institutes of Health (Bethesda, USA) on human spinal cord neurophysiology. He is a Professor at the University of São Paulo where he directs the Biomedical Engineering Laboratory of the School of Engineering (EPUSP). His current interests are in computational neuroscience, neural control of human motor activities and biomedical signal processing. A specific interest is the development of a computer simulator of neuronal networks of the spinal cord that could be used by biomedical scientists studying the nervous system involved in motor control.

Please cite this article as: M.F. Vieira, A.F. Kohn, Compartmental models of mammalian motoneurons of types S, FR and FF and their computer simulation, Comp. Biol. Med. (2006), doi: 10.1016/j.compbiomed.2006.09.001